fuels

MDPI

Article

The Effect of Ambient and Injection Pressure on Droplet Size of Ammonia Sprays in a Constant Volume Chamber

Li Shen and Felix Leach *

Department of Engineering Science, University of Oxford, Parks Road, Oxford OX1 3PJ, UK; sam-li.shen@eng.ox.ac.uk
* Correspondence: felix.leach@eng.ox.ac.uk

Abstract

Ammonia, a zero carbon energy vector, is under consideration for decarbonising marine and energy storage applications due to its high mass-based energy density compared to many alternatives. In addition, there is widespread existing supply and transportation infrastructure due to ammonia's use as a fertiliser. When injected in its liquid form, however, ammonia behaves quite differently to traditional fuels due to its high saturation pressure and enthalpy of vaporisation, amongst other things. This means that fundamental data on ammonia sprays need to be collected in order to understand ammonia spray behaviour and calibrate models of ammonia sprays needed for design in the virtual world. Previous work on ammonia sprays has mostly focused on spray morphology at a macroscopic level (such as liquid penetration length). However, there are fewer studies of ammonia sprays at a microscopic level. In this study, liquid ammonia was injected into a constant-volume chamber using a direct injector at two injection pressures (100 bar and 150 bar) and a range of ambient pressures from 3–13 bar. This range of ambient conditions spans regimes from flash-boiling to non-flash-boiling, thereby enabling systematic investigation of the transition between these regimes. A laser diffraction technique was used for measuring the droplet sizes of the spray at different locations (in a cylindrical volume with a diameter of 10 mm) within the spray plume at 10 kHz, and the nominal droplet sizes were quantified by the Sauter Mean Diameter (SMD). These SMD values provided, at a microscopic level, an insight of the atomisation of the spray as it left the nozzle and penetrated into an environment with different densities. It was found that the tested injector leads to a breakup dominant spray behaviour with liquid ammonia and hence the SMD values decrease as ambient pressure increases. In addition, the droplets are generally smaller at the outer edge of the spray plume compared to the inner part and both the injection pressure and injection duration have a strong effect on the droplet sizes.

Keywords: ammonia; spray; droplet size; sauter mean diameter

Academic Editor: Isaac K. Gamwo

Received: 31 October 2025
Revised: 30 January 2026
Accepted: 9 March 2026
Published: 12 March 2026

1. Introduction

Maritime transport, despite having experienced significant reductions in carbon dioxide emissions on a per-ton basis recently, emits over 1 billion tonnes of carbon dioxide each year [1], which represents ≈2.9% of the global total anthropogenic greenhouse gas emissions per year. Ammonia (NH_3), a carbon-free energy vector, is a serious candidate to decarbonise this sector alongside the energy storage sector [2]. Ammonia is a particularly strong candidate for this due to the widespread availability of existing infrastructure and

safe-handling procedures as well as its high energy density among carbon-free fuels, approximately 10 times greater than lithium-ion batteries and around 30% higher than liquid hydrogen [3]—indeed it has about 50% more hydrogen by volume compared to liquid hydrogen [4,5]. Ammonia is already produced in large quantities—176 million tonnes in 2019 [6].

Initial research into ammonia energy using reciprocating engines has focussed on gaseous ammonia injection [7–9]. Gaseous injection offers several advantages, including improved local air–ammonia mixing, mechanical simplicity, and the potential to reuse existing natural gas engine technologies [10]. However, gaseous injection, especially when implemented as port fuel injection, significantly reduces both the power density and volumetric efficiency of internal combustion engines [11].

Directly injecting liquid ammonia into the cylinder presents a promising alternative that leverages the higher momentum of liquid droplets to enhance global air–fuel mixing—an important factor influencing combustion efficiency and emissions formation [12]. Additionally, liquid injection enables a substantially higher power density due to the much greater density of liquid ammonia (≈850 times higher than the gaseous phase). Nonetheless, liquid ammonia introduces new challenges: its high latent heat of vaporisation hampers evaporation within the combustion chamber, leading to incomplete vaporisation, reduced combustion efficiency, and elevated emissions. These limitations underscore the need for a more thorough understanding of the breakup and evaporation behaviour of liquid ammonia sprays under engine-relevant conditions.

Several recent studies have begun to explore these challenges using repurposed gasoline direct injection (GDI) injectors. Pele et al. [13], showed that ammonia sprays exhibit markedly different behaviour compared to ethanol and gasoline sprays, including longer penetration lengths, smaller spray cone angles, and a stronger dependence on ambient conditions. Cheng et al. [14] observed that ammonia sprays exhibited wider spray cone angles than methanol or ethanol sprays and had higher ammonia-air mixing, again showing high sensitivity to ambient pressure and temperature. Colson et al. [15] identified a controllable transition into flash-boiling conditions that depended on nozzle geometry, highlighting the complex thermofluidic behaviour of ammonia. This study's authors investigated the macroscopic ammonia spray characteristics of a 6-hole GDI injection (the same injector as used in this work) at a variety of flash-boiling and non-flash-boiling conditions [16]. They found that the ambient-to-saturation pressure ratio was a very important parameter to describe the behaviour of the ammonia sprays and that the spray characteristics could be divided into three regions: a drag dominant region (at high ambient pressures), an evaporation dominant region (at medium ambient pressures) and a spray collapse region (at low ambient pressures). This study represents an extension of this work from the macroscopic to the microscopic domain.

Beyond GDI systems, Fang et al. [17], using a repurposed diesel injector at significantly higher injection pressures (up to 1000 bar), demonstrated that under flash-boiling conditions—where the ambient pressure falls below the saturation pressure of ammonia—the penetration velocity of the spray tip decreases substantially. Together, these studies indicate that ammonia spray behaviour is strongly influenced by both injection and ambient conditions, and that existing models derived from hydrocarbon or alcohol fuels may not adequately describe ammonia's complex two-phase dynamics.

This growing body of work underscores the necessity of systematic experimental investigations of liquid ammonia sprays under controlled, engine-relevant conditions. Such studies are critical to understanding the fundamental physics of ammonia evaporation and mixing, and to support the development and validation of predictive spray models tailored to ammonia.

All of the studies mentioned in the previous paragraph have been exploring the macroscopic characteristics of ammonia sprays using some form of imaging, for example Schlieren or backlit techniques. Fewer studies have explored microscopic characteristics such as Sauter Mean Diameter (SMD)—an important parameter for assessing spray breakup. Zhong et al. [18] used backlit imaging with a suitable lens to evaluate SMD from ammonia sprays from a diesel injector but were restricted on the minimum SMD they could measure by their lens. They found that average SMDs were between 20 and 30 µm for almost all the cases they tested. Recent work by this study's authors using a single hole, outward opening injector examined the characteristics of ammonia sprays both microscopically and macroscopically [19]. It was found that ammonia sprays experienced transition into flash boiling, and the ambient conditions caused substantial change in both the ammonia spray morphology and the SMD values. Zembi et al., using the same instrument as used in this work, measured a three-fold difference in SMD using the ECN Spray M single-hole injector between a single flashing and non-flashing condition [20]. Liu et al. used a Phase Doppler Particle Analyzer (PDPA) to measure SMD from a single hole injector at injection pressures between 600 and 1200 bar under flash boiling and non-flash boiling conditions. They reported a 65% change in SMD between these two regions [21]. Liu et al., using a single-hole Bosch diesel injector and Particle Droplet Image Analysis (PDIA), again saw a near-doubling of SMD moving from flash boiling to non-flash boiling conditions [22]. Liu et al. [23], again using PDIA, measured ammonia spray SMD at an injection pressure of 10 bar (suitable for port injection but not direct injection). They reported SMDs between 10 and 20 µm alongside substantial variation in SMD with ambient conditions. There remain, however, significant unanswered questions on ammonia sprays, particularly with regard to understanding different injector and nozzle designs (notably multi-hole injectors) as well as how SMD and morphology might change during breakup at different locations within the same spray from a multi-hole injector with interacting spray plumes. This work aims to answer the latter question.

In this paper, liquid anhydrous ammonia was injected from a repurposed multi-hole GDI injector into a constant volume chamber filled with nitrogen gas. The ambient (chamber) pressure varied from 3–13 bar, the injection pressure was set to 100 bar and 150 bar, the injection duration was 1 ms and 2 ms. The resulting ammonia sprays were recorded by backlit images and the droplet size within the spray plume was measured using laser diffraction at 10 kHz in three different measurement regions.

2. Materials and Methods

2.1. TestRig

Measurements of liquid ammonia sprays were conducted in a constant-volume chamber filled with nitrogen gas at various ambient pressures. The design and operation of this chamber have been described in detail in previous work [16,19]; however, a concise summary is provided here for completeness. The chamber allows optical access along three orthogonal axes through five fused silica (quartz) windows (Newcastle Optical Engineering, Wallsend, UK) of 80 mm viewable diameter—two pairs positioned laterally and one window at the bottom—enabling high-quality optical diagnostics of the spray development process. A schematic of the rig showing the general arrangement and the optical diagnostics is shown in Figure 1. This shows the axes referred to in later figures, with the camera and laser droplet sizer (described in later paragraphs) imaging simultaneously on orthogonal axes, both orthogonal to the vertically mounted injector.

The injector employed in this study was a BOSCH (Robert Bosch, Schwieberdingen, Germany) six-hole gasoline direct injector (GDI), originally designed for a production vehicle combustion system but subsequently modified for operation with liquid anhydrous

ammonia. This injector has been characterised in previous studies, including a macroscopic study with ammonia [16,24,25]. This work is the first characterisation of this injector in the microscopic domain. It exhibits a distinctive spray geometry, consisting of four axially oriented plumes directed downwards and two additional plumes oriented more radially (in this work, plume refers to a single jet leaving the nozzle and spray refers to all of the plumes together). Of note is that this injector, having six holes, will exhibit plume-to-plume interactions, which have been observed in previous work with this injector [16]. Given many 'real world' applications use multi-hole injectors, it is important to study them so that the effect of these interactions on the results can be observed. The injector was actuated using a manufacturer-supplied driver. Control of the injection duration and synchronisation between the injector, high-speed camera, and laser droplet sizing system was achieved via a BNC 725 pulse/delay generator (Berkeley Nucleonics Corporation, San Rafael, CA, USA), ensuring precise temporal coordination of all measurement systems.

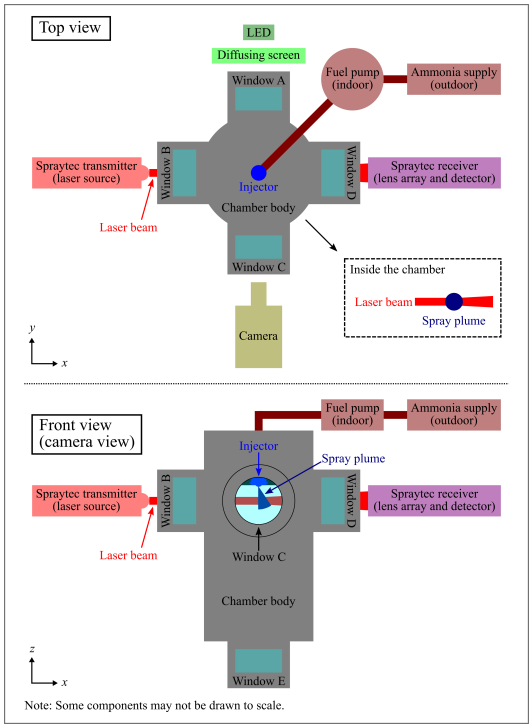

Figure 1. Schematic of the test rig showing the general arrangement and the optical diagnostics.

Anhydrous ammonia was pressurised using a GX40 series pneumatic pump (Heypac, Aldershot, UK) before being delivered to the injector. The fuel supply line pressure was monitored by an in-line 3100 series transducer (Gems Sensors & Controls, Plainville, CT, USA). Chamber pressure, set and maintained using nitrogen gas, was measured using an identical Gems 3100 series transducer mounted on the chamber wall. All signals—including those from pressure sensors, injector triggers, and synchronisation pulses—were recorded using a PicoScope 6000E series data acquisition system (Pico Technology, St. Neots, UK) operating at a sampling frequency of 100 kHz. The laser droplet sizer system employed a dedicated data logger to ensure optimal temporal and spatial resolution of droplet size measurements.

Optical diagnostics of the sprays were performed using a high-speed imaging system and a laser-based droplet sizing instrument. The imaging system consisted of a FASTCAM-1024PCI 100K high-speed camera (Photron, Tokyo, Japan) operating at 10,000 FPS with a spatial resolution of 256 pixels × 272 pixels. Shadowgraph images were acquired by back-illuminating the spray using a broadband white LED light source directed through a

diffusing screen to provide uniform illumination across the field of view. This arrangement enabled clear visualisation of the macroscopic spray structure, with a spatial resolution of approximately 0.25 mm pixels^{-1}.

This experimental configuration enabled simultaneous high-speed imaging and droplet sizing measurements, allowing detailed characterisation of the ammonia spray morphology and its response to variations in injection and ambient pressure conditions.

The laser spray droplet sizer used was a Spraytec device (Malvern Panalytical, Malvern, UK) [26], which uses the laser diffraction technique to measure particle size at the same sampling frequency as the high speed images (i.e., at 10 kHz). The Spraytec was used with a 300 mm lens allowing droplets 0.1–900 µm to be measured. Laser diffraction provides a line-of-sight integration of the bulk properties of the spray through a column defined by the laser beam diameter (in this case a 632.8 nm collimated beam from a helium-neon laser with diameter ≈ 10 mm). When the beam interacts with the spray, it is scattered by individual droplets, with smaller droplets usually scattering light at a larger angles. In this work, a substantial proportion of the test points are at flash boiling conditions, because the Spraytec instrument is measuring light scattering, which is caused by the vapour-liquid interface, it is not thought that flash boiling will influence this. This is then measured by a series of concentric photodiode detector elements and is processed into a droplet size distribution. From that distribution, the Sauter Mean Diameter (SMD) [27–29] can be calculated. In this work, for reasons of confidentiality, the droplet distributions have then been rescaled by dividing by a nominal value—the same nominal value for all test points.

2.2. Test Conditions

The test points in this paper were taken at two injection pressures (100 bar and 150 bar), two injection durations (1 ms and 2 ms), three droplet size measurement regions, and a range of ambient pressures (from 3–13 bar with 2 bar increments). These conditions were chosen to span three regions which macroscopic studies had revealed different behaviours of ammonia sprays [16]. These regions are a drag dominant region (at high ambient pressures), an evaporation dominant region (at medium ambient pressures) and a spray collapse region (at low ambient pressures)—these could also be understood as non-flash boiling, transition flashing, and full-flash boiling. Such conditions, will be encountered during real internal combustion engine operation with the low pressures corresponding to earlier injection and the higher pressures later injection in the compression stroke. A list of the test points is provided in Table 1. Figure 2 shows an image taken by the high speed camera prior to injection, and the three cylindrical droplet size measurement regions are marked using colored rectangles (on the camera view) and circles (on the side view). The injector was mounted such that its hole pattern was symmetric with respect to the $y = 0$ plane. Each measurement region is a cylinder whose diameter is about 10 mm (beam diameter), and whose length is the distance between the laser emitter and the detector of the Spraytec device. These regions corresponded to different locations in the plume—the centre of region A is 26.5 mm below the injector tip and on the symmetrical plane of the injector holes, to capture the droplet sizes near the spray centreline; the centre of region B is 25 mm away from the centre of region A (in the y direction) and hence this region was away from the spray centreline, to enable the measurement of droplet sizes at the outer edge of the plume; the centre of region C is 10 mm lower (in the z direction) than the centre of region A, and in this region the measurement is further downstream and closer to the spray tip. Figures 3–5 illustrate that the results of this technique is an integrated line-of-sight measurement that at different times during the injection will correspond to different parts of the spray plume(s).

Table 1. List of Test Points.

Run No. *	Injection Pressure (bar) †	Ambient Pressure (bar) †	Injection Duration (ms)	Measurement Region ‡
1–6	150	3, 5, 7, 9, 11, 13	1.0	A ($y = 0$, $z = -26.5$ mm)
7–12	150	3, 5, 7, 9, 11, 13	1.0	B ($y = 25$, $z = -26.5$ mm)
13–18	100	3, 5, 7, 9, 11, 13	1.0	B ($y = 25$, $z = -26.5$ mm)
19–24	150	3, 5, 7, 9, 11, 13	1.0	C ($y = 0$, $z = -36.5$ mm)
25–30	150	3, 5, 7, 9, 11, 13	2.0	C ($y = 0$, $z = -36.5$ mm)
31–33	100	5, 9, 13	1.0	C ($y = 0$, $z = -36.5$ mm)
34–36	100	5, 9, 13	2.0	C ($y = 0$, $z = -36.5$ mm)

* For each test run, the injector was triggered at 1 Hz for 20 consecutive shots. † All pressure values in this manuscript are reported in absolute pressure units. ‡ The coordinates reported here refer to the centre of the beam, see Figure 2 for details.

At each point, the injector was triggered at 1 Hz to perform 20 consecutive shots. After each test, the chamber was vented completely and purged using nitrogen gas for at least two minutes, before it was recharged by nitrogen gas to the target ambient pressure for the next test point.

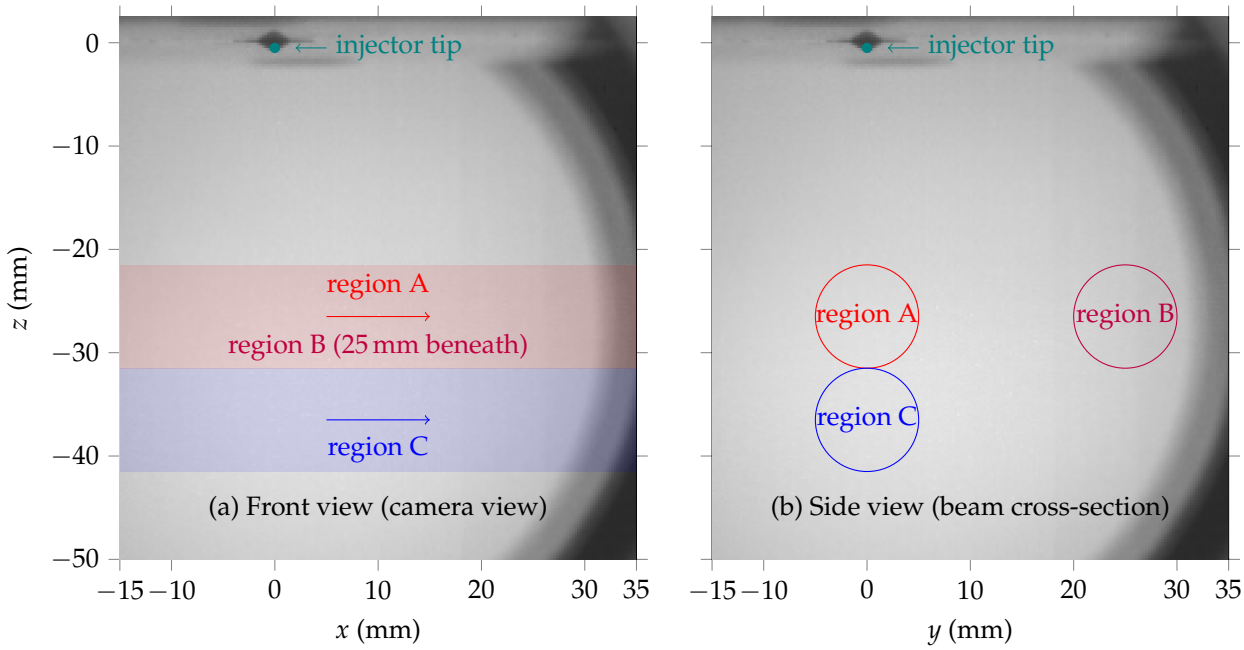

Figure 2. Regions in which the droplet size measurement were taken, shown in a blank image (i.e., camera view) taken before the test in (**a**). In order to illustrate the location of the beam in a side view, the beam cross-section is superposed on the same image in (**b**). The beam diameter was about 10 mm. The centre of the beam in each region is provided in Table 1. The tip of the six hole injector points downwards (along the negative z direction), and its hole pattern is symmetric with respect to the $y = 0$ plane (three holes on either side).

2.3. Sauter Mean Diameter (SMD) Calculation

At each sampled instant, the Spraytec software turns the scattered signals from the droplets into a volume-based size distribution, which can be illustrated by a histogram such as Figure 3. The horizontal axis, on a log scale, shows the bins edges of the histogram (droplet sizes), and the vertical axis reports the volumetric partition of each bin, normalised by the total volume of the droplets within the measurement region.

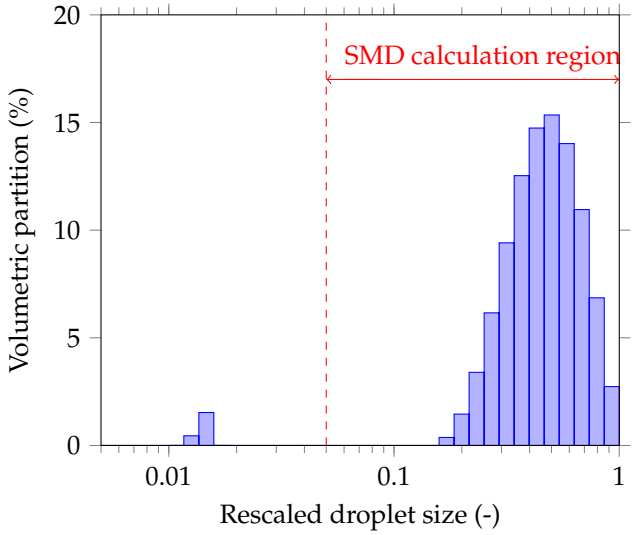

Figure 3. An example droplet size distribution measured by the Malvern Spraytec device.

Based on Figure 3, at this example instant, the majority of droplets falls into the rescaled range from 0.1–1, and their sizes are grouped into a somewhat Gaussian distribution shown in the histogram. However, in addition to this expected distribution, there is a small portion of "droplets", distinct from the bulk signal, falls into the rescaled bins at around 0.012. Such a phenomenon seems to be non-physical—despite the fact that the evaporation and breakup processes of droplets are complex, one would expect the droplet size distribution to be at least continuous (non-zero bins should be grouped together). After carefully checking the experimental setup (including taking measurements without injection), it was found that the quartz windows of the chamber created a diffraction pattern at a fixed angle, and such a pattern created a phantom signal manifesting itself as droplets at around 0.012 rescaled value.

Using the quartz windows was necessary to maintain the chamber pressure while providing the optical access for the measurement, and given that the amount of the phantom signal was insignificant (less than 2% of the total volume) and was at a substantially lower diameter compared to all other droplets, any signal below 0.05 was discarded prior to calculating the SMD. This value was chosen as, on consulting Figure 3, it is clear that any value between say 0.03–0.1 will achieve the necessary outcome of removing the phantom signal. As a result, the SMD values computed in the Spraytec software cannot be used directly. The SMD values reported in this paper were instead calculated in MATLAB r2021b from the droplet size distribution exported from the Spraytec software, by considering only the bin values within the SMD calculation region shown in Figure 3 and using the formula below:

$$\mathrm{SMD} = \frac{\sum\left(n_i \cdot d_i^3\right)}{\sum\left(n_i \cdot d_i^2\right)} \tag{1}$$

where d_i is the geometric mean diameter of the i-th bin and n_i is the number-based partition of this bin, whose value can be converted from a volume-based distribution such as Figure 3. Although the actual formula was not explicitly written in the Spraytec manual [26], the formula above can be inferred from the manual and it was checked that the result of this in-house MATLAB r2021b algorithm computes the same SMD value as the software, if the entire distribution were used. After accounting for the signals within the SMD calculation region only, the resulting SMD value for a distribution in Figure 3 is 0.432 (instead of 0.239 if the whole distribution were used).

2.4. Data Analysis

In each measurement region shown in Figure 2, the beam was located a few tens of millimeters away from the injector tip, so it would take some time for the spray to penetrate into the corresponding measurement region. This is perhaps best seen in Figures 4 and 5, which show an example set of spray images on two orthogonal planes at two times after end of injection. It is of note that these images are not taken simultaneously due to limitations with the set-up, but are achieved by rotating the injector by 90°. They should be viewed as representative but, of course, shot-to-shot variations prevent a direct side-by-side comparison. Based on its distance away from the injector tip, the timing at which the spray enters each measurement region may be different. For instance, as shown in the backlit images taken at an example test point (Run 2 in Table 1) in Figures 4 and 5a, at 0.7 ms aSOI, the spray has just entered measurement region A, but has not yet reached measurement region C. And it was not until at 1.1 ms aSOI (Figure 4b) that the spray entered region C—and at this time, only the plumes from the four 'downward' facing nozzles have reached region C, the more radial plumes still not having reached that region, and only just having reached region A.

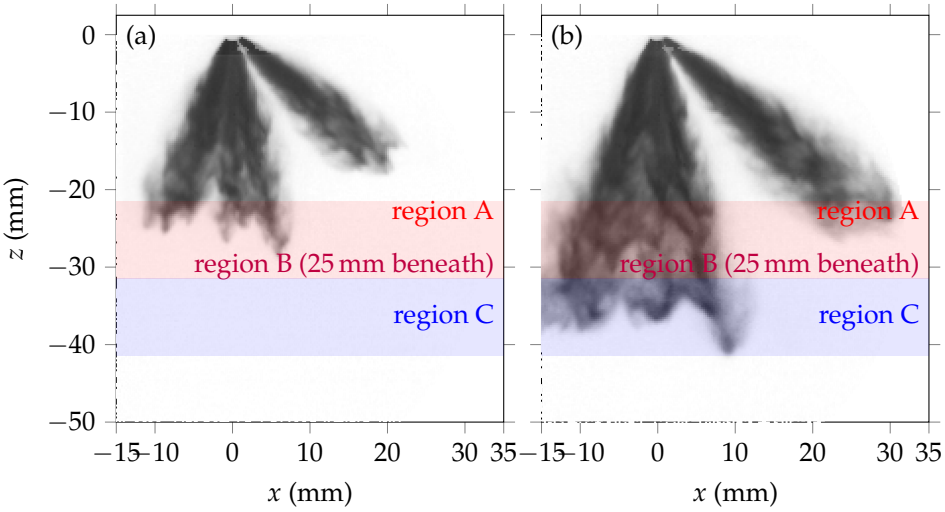

Figure 4. Example backlit images taken in the x-z plane at a 5 bar ambient pressure test point (Run 2 in Table 1). (**a**) At 0.7 ms aSOI and (**b**) at 1.1 ms aSOI.

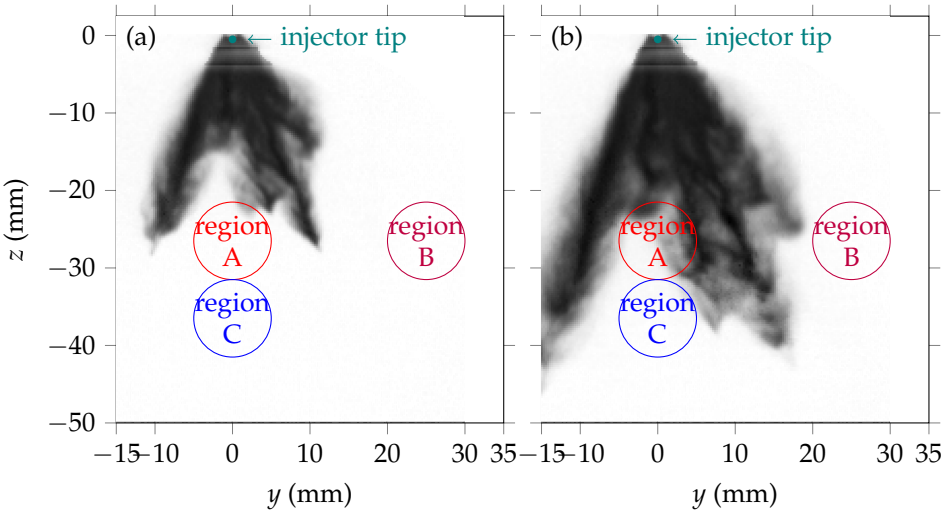

Figure 5. Example backlit images taken in the y-z plane at a 5 bar ambient pressure test point (Run 2 in Table 1). (**a**) At 0.7 ms aSOI and (**b**) at 1.1 ms aSOI.

In addition to the scattered light from the droplets, the Spraytec device also collected the un-scattered light and reported the value as the transmission of laser energy [26]. When the droplets entered the measurement region, the transmission would drop rapidly since the amount of un-scattered light was reduced by droplets scattering the incoming beam. This provides an indication of whether the spray has entered measurement region and whether there are sufficient numbers of droplets to ensure an accurate measurement [19,26]. Before interpreting any droplet size data, a start measurement timing needs to be selected based on the transmission value. The reduction in transmission will also effect the accuracy of the instrument because with a high droplet density, the high number of droplets will lead to high levels of multiple scattering which will reduce the accuracy [30]. However, in this application, the multi-scattering correction from the manufacturer provided post-processing software was used, which is shown to reduce this effect [26]. Nevertheless, this is a well-documented limitation of the technique used [30], and the results should be interpreted with this in mind.

In this experiment, raw transmission values reported by Spraytec varied significantly in different measurement regions—the minimum transmission value recorded in region A at a certain instant could be much lower than the ones of region B and region C, since the latter two were further away from the injector tip (see Figure 2) and fewer droplets passed through the beam in these regions. In order to use a universal cutoff for the transmission value, for each test run, the raw transmission values (%T) reported in Spraytec were first normalised into a range of 0 to 1, using the formula below:

$$\text{relative transmission} = \frac{\%T - \min \%T}{\max \%T - \min \%T} \times 100\%$$

The results in two regions (region A and region C, see Figure 2) and under three ambient pressures (5 bar, 9 bar and 13 bar) are shown in Figure 6 as a function of timings after the start of injection (aSOI). The same injection pressure (150 bar) and duration (1.0 ms) were used in these tests (Runs 2, 4, 6, 20, 22 and 24 in Table 1). At 5 bar ambient pressure, the sprayspray tip first reaches region A at about 0.7 ms aSOI (see image in Figure 4a), and the relative transmission (blue circles in Figure 6) dropped rapidly within the next 0.8 ms as more droplets entered the measurement region (see, for instance, an image recorded at 1.1 ms aSOI in Figure 4b). After the relative transmission reached its minimum value, and the feed from the injector had also stopped, the remaining spray gradually evaporated within the chamber. This led to a slow increase in relative transmission after 1.5 ms aSOI in Figure 6 as fewer droplets are present in the measurement region.

A similar trend can be observed in other measurement regions as well, albeit that under the same ambient pressure (5 bar), the spray entered region C at a slightly later timing (at about 1.1 ms aSOI), as indicated by the image (Figure 4b) and transmission data (blue hollow circles in Figure 6), since region C was further downstream and away from the injector tip (see Figure 2). In the same measurement region (for instance in region A), when the ambient pressure was higher (red squares for 9 bar and teal triangles for 13 bar in Figure 6), the spray also entered the measurement region later than the 5 bar condition (blue circles) since the higher ambient resistance in these conditions prevented the spray from penetrating as fast as it would have at lower ambient pressures.

These similar trends enabled a universal cutoff for the timing of interest based on relative transmission, and after cross checking with raw spray images, the cutoff threshold was selected to be 25%. In other words, when the relative transmission dropped below 25%, it was considered that the majority of the spray had entered the measurement region, which was evident from the spray images, to produce a reliable droplet size distribution for computing the SMD.

Based on this cutoff threshold of the relative transmission, the measurement start timing of each test condition will be different. For example, at 5 bar ambient pressure, the start measurement timing of region A (blue circles in Figure 6, image shown in Figure 4b) was 1.1 ms aSOI and of region C (blue hollow circles in Figure 6, images not shown for brevity) was 1.6 ms aSOI. Such a difference reflects an actual scenario of whether there were enough droplets within each measurement region to obtain a robust and relevant SMD measurement (there must be spray in the region for the SMD values to be relevant). As can be seen in Figure 6, the SMD average values obtained will be relatively insensitive to the actual choice of start timing because the gradient of the relative transmission slope is steep and so the precise time at which the 25% threshold is passed will be a matter of only one or two data points relative to the spray duration—the same portion of the spray will always be being captured.

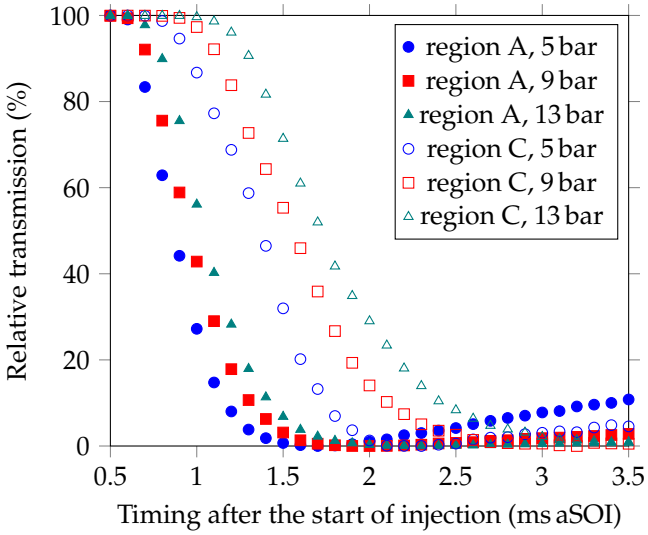

Figure 6. Relative transmission (amount of un-scattered light) recorded at two measurement regions and under three ambient pressures as a function of timing after the start of injection. All the tests were performed at an injection pressure of 150 bar and an injection duration of 1.0 ms (Runs 2, 4, 6, 20, 22 and 24 in Table 1).

3. Results

3.1. Temporal Evolution of SMD and the Time-Based Average

Figure 7 shows the rescaled Sauter Mean Diameter as a function of timings after the start of injection at three ambient pressures (blue dots for 5 bar, red squares for 9 bar and teal triangles for 13 bar). The data was recorded in measurement region A (see Figure 2), and these tests were all performed with an injection pressure of 150 bar and an injection duration of 1.0 ms (Runs 2, 4 and 6 in Table 1). At the 5 bar test point (blue dots in Figure 7), the SMD first dropped from around 0.9 to about 0.8 within the first 0.5 ms and stayed at the smaller value for about 0.2 ms, until the value increased gradually and stabilised at around 0.93 At higher ambient pressures, despite the corresponding start timings for the measurement being different (higher ambient resistance led to a retarded start timing), the trends of temporal evolution of SMD are similar to the 5 bar test point.

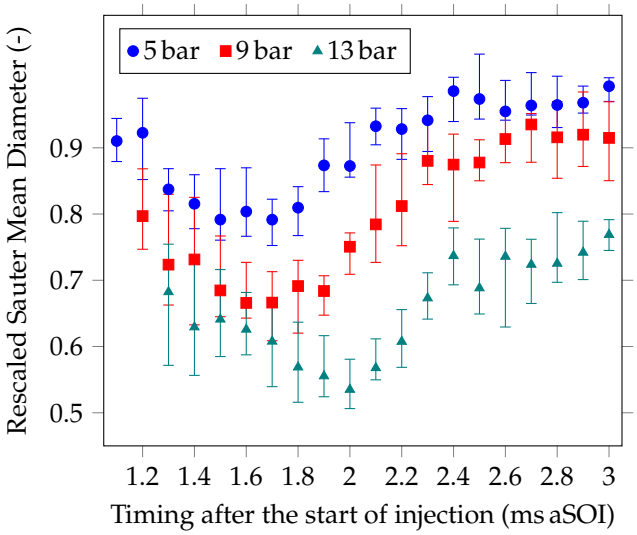

Figure 7. Rescaled Sauter Mean Diameter measured at different ambient pressures as a function of timings after the start of injection. All the tests were performed in measurement region A, under an injection pressure of 150 bar and an injection duration of 1.0 ms (Runs 2, 4 and 6 in Table 1). The markers show the median value of 20 consecutive shots, and the error bars bound the middle two quartiles.

It is important to note that the spray from the six-hole injector was in motion while the measurement beam was fixed in space, so different parts of the spray or plumes from different nozzles may be measured at each instant. Again for the 5 bar test point (blue dots in Figure 7), by the start timing that SMD value was reported (at 1.1 ms aSOI), the plumes from the four axial (downward pointing) nozzles had well entered in this measurement region (see Figure 4b), and only the front part the plumes (plume tip) from the two radial (side pointing) nozzles were captured. There were two physical phenomena happening, each of which led to an opposing temporal trend in SMD after this start timing. The evaporation and breakup of the droplets within the four axial plumes would result in smaller droplets and hence a decreased SMD at a later timing. On the other hand, at the rear of the two radial plumes (plume body), the SMD could increase, as usually the plume body contains larger droplets than the plume tip due to a weaker ambient gas entrainment preventing evaporation and breakup from occurring. The initial drop in SMD observed in Figure 7 was likely caused by the former phenomenon (droplet evaporation within the axial plumes), but as the more and more larger droplets from the radial plumes entered the measurement region, the latter phenomenon became more dominant and eventually caused an increase in SMD.

Despite the observations made in Figure 7 indicating that a temporally resolved SMD measurement is possible and can be, to some extent, interpreted by checking the raw images, the instantaneous droplet size measurement for fuel sprays using the Spraytec is prone to be influenced by actual flow conditions—the shot-to-shot variation, quantified by the error bars in Figure 7, was huge (almost 20% of the absolute value). Also, for the examination of the atomisation quality across the entire spray under different test conditions, it was unnecessary to keep the temporal resolution of the SMD. Instead, it was recommended by the manufacturer [26] that, for a fuel spray application such as this paper, a time-based average should be performed to generate the SMD for a plume passing through the measurement region over a timed interval. Therefore, henceforth, for each shot, SMD values will no longer be reported at each sample instant (at 10 kHz), but instead reported as a time-based averaged value. Such an averaged SMD, for any given shot, was obtained by the following procedure:

1. Average the raw scattered data in the Spraytec software over a selected timed interval;
2. Compute a droplet size distribution based on the averaged scattered data using the Spraytec software;
3. Process the resulting droplet size distribution in MATLAB to generate the SMD value.

Unless otherwise mentioned, the length of the averaging interval was chosen to be the same as the injection duration of that shot. The starting time of the average can vary based on test conditions and comparison targets. For instance, if the front part of the spray were of interest, the timed interval for the 5 bar test point in Figure 7 could be from 1.1 ms aSOI (start timing of measurement), lasted for the injection duration of that shot (which is 1.0 ms), to 2.1 ms aSOI. More examples of the time-averaged SMD values will be discussed in the following sections.

3.2. Droplet Size Measured at Different Regions and Ambient Pressures

Figure 8a shows the SMD values measured at different regions, as a function of ambient pressures. All of the tests were performed at an injection pressure of 150 bar and an injection duration of 1.0 ms (Runs 1–6, 7–12 and 19–24 in Table 1). The exact measurement regions are shown in Figure 2. In order to provide a comparison of the droplet sizes measured in different regions, it was necessary to select a common start timing (and hence a common timed interval) for performing the time-based average at each ambient pressure when reporting the SMD values. Such a common timing needs to be late enough to allow sufficient numbers of droplets entering all the three regions, hence the latest among the three start measurement timings was selected. For instance, at 5 bar ambient pressure conditions (Runs 2, 8 and 20 in Table 1), the start measurement timings were 1.1 ms aSOI for measurement region A, 1.7 ms aSOI for region B and 1.6 ms aSOI for region C, so their common start timing for computing the time-averaged SMD was from 1.7 ms aSOI, and the common time interval was therefore from 1.7 ms aSOI to 2.7 ms aSOI. The choice of a common interval enables the examination of droplet sizes for different parts of the spray (despite the measurements being in different test runs), and the spray image recorded for one shot at the common start measurement timing (1.7 ms aSOI) is provided in Figure 8b for reference.

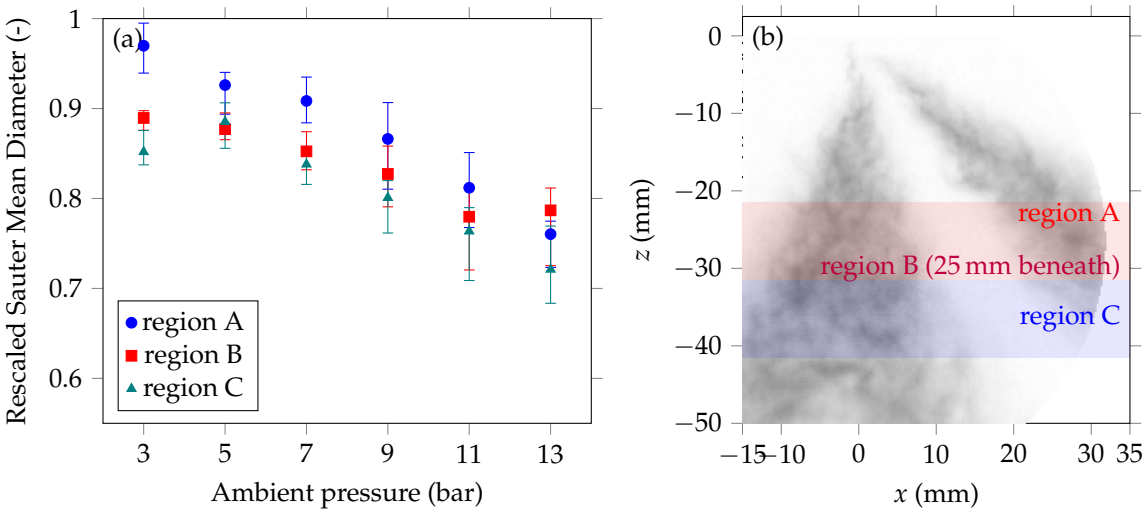

Figure 8. Rescaled (**a**) Sauter Mean Diameter measured in different regions within the spray as a function of ambient pressures. All the tests were performed at an injection pressure of 150 bar and an injection duration of 1.0 ms (Runs 1–6, 7–12 and 19–24 in Table 1). The markers show the median value of 20 consecutive shots, and the error bars bound the middle two quartiles. (**b**) An example backlit image taken at 1.7 ms aSOI of a 5 bar ambient pressure test point (Run 2 in Table 1).

From Figure 8, it can be seen that in each region, the SMD values generally decrease as ambient pressure increases. Such a trend indicates that for the injector used in this work, after the spray leaves the nozzle, breakup induced by drag (or resistance from the ambient gas) dominates the droplet forming process, and as a result, higher ambient resistance (i.e., ambient pressure) leads to smaller droplets. On the other hand, in previous work using a different injector, but otherwise the same experimental setup [19], it was observed that when the droplet forming process was evaporation dominated, an opposite trend can occur, where a lower ambient pressure leads to smaller droplets. A closer look at Figure 8 shows that the error bars are wider at higher ambient pressure conditions. This further indicates that at higher ambient pressure, the increased drag between the high speed spray plume and the quiescent ambient gases leads to greater turbulence (particularly at the plume edges) and hence a more complex and faster breakup process. Hence, one would expect the shot-to-shot variation to be larger. When considering applications of these sprays to internal combustion engines, such variability would lead to variations in mixture preparation cycle-to-cycle in an engine and this would likely lead to variations in combustion stability—a link well documented in the literature [31].

Notably, such a competition between resistance-induced breakup and evaporation to due low pressure caused a flipped trend at low ambient pressures in region C (teal triangles in Figure 8)—the SMD value at 3 bar ambient pressure was 0.04 lower than the one at 5 bar ambient pressure. This means when ambient pressure is low enough and enters the flash boiling regime, more droplets start to breakup internally (induced by the flash boiling phenomenon [32]), this competing breakup mechanism can overtake the resistance-induced breakup (breakup due to drag) and lead to smaller droplets. Such a phenomenon is less obvious when the measurement region was closer to the centre and more upstream of the radial plume (such as region A, the blue dots in Figure 8), potentially because there was not enough energy from the surrounding ambient gases to support the flash boiling in this region (due to ammonia's very high enthalpy of vaporisation).

Comparing the droplet sizes in different measurement regions, from Figure 8, at the same ambient pressure, the droplets are larger at the centre of the spray plume (region A, blue dots) compared to at the outer edge (region C, teal triangles), as a result of the ambient gas entrainment promoting the droplet breakup near the outer edge. The droplets further downstream of the spray plume (region B, red squares) are also generally smaller than upstream (region A), since these droplets left the nozzle earlier and have had more time than the following droplets to evaporate and breakup. These droplets also do not benefit from the "platooning" effect experienced by the droplets which follow in their wake.

3.3. Effect of Injection Pressure

Figure 9 shows the SMD values measured at different injection pressures as a function of ambient pressures. Figure 9a shows values measured in region B (on the side of the spray near the outer edge, see Figure 2), and Figure 9b shows values measured in region C (near the spray tip). All of the tests were performed with an injection duration of 1.0 ms. The start timing for the time-based average was selected to be the same as the start timing of measurement, so that the SMD results better represent the initial droplets entering each measurement region. In terms of ambient pressure, a similar trend to that already seen can be observed, that the SMD values are lower at higher ambient pressure conditions.

When the injection pressure is higher (at 150 bar, blue dots in Figure 9a and teal filled squares in Figure 9b), at each ambient pressure, the SMD values are generally lower (up to 12% lower, with the highest differences observed at the highest ambient pressures) compared to the values at a lower injection pressure (at 100 bar, red hollow circles in Figure 9a and orange hollow squares in Figure 9b). At higher injection pressure, the

momentum of the spray generated from the nozzle was larger, leading to a larger plume speed relative to the quiescent ambient gas. This further enhanced the interaction between the spray and ambient gas, and promoted the droplet formation and breakup, leading to smaller droplets and hence a lower SMD value. It is also probable that at higher injection pressures, there is greater in-nozzle cavitation leading to greater breakup, although this cannot be verified with the current measurements.

Compare two plots in Figure 9, the differences in terms of droplet sizes are more obvious in region C compared to in region B, showing that the injection pressure has a stronger effect on the droplet size nearer to the spray tip. Also, such an effect is larger when ambient pressure is higher—as observed in both plots in Figure 9, the difference between SMD values of the two injection pressures gradually increases as ambient pressure increases. At 3 bar and 5 bar in region B (Figure 9a), the SMD values corresponding to the two different injection pressures are almost the same, showing that at low ambient pressure when the drag is small, changing the injection pressure has a minimal effect on the droplet size.

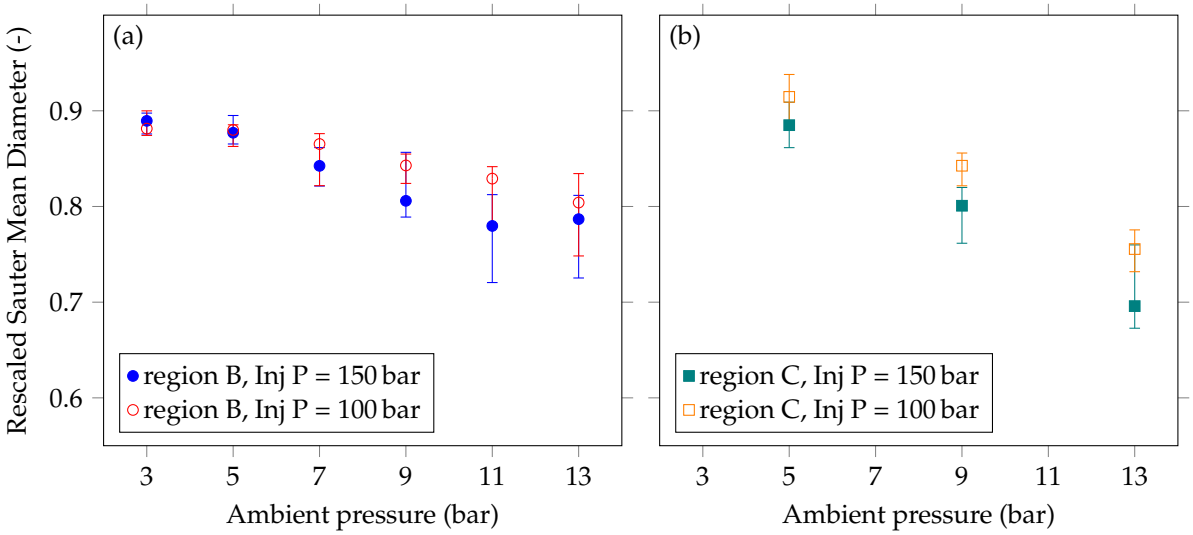

Figure 9. Rescaled Sauter Mean Diameter measured at different injection pressures as a function of ambient pressures in two regions—(**a**) region B and (**b**) region C. All the tests were performed at an injection duration of 1.0 ms (Runs 7–18, 20, 22, 24 and 31 in Table 1). The markers show the median value of 20 consecutive shots, and the error bars bound the middle two quartiles.

3.4. Effect of Injection Duration (Ambient Gas Motion)

For these tests, the previous approach of setting the length of the averaging time interval to be the same as the injection duration of that shot would not lead to a fair comparison as the averaging window would not be the same for each test. At any fixed combination of injection and ambient pressures, the start measurement timing is the same, irrespective of the length of the injection duration, since the spray tip will always reach the measurement region at the same time. However, to perform the time-based average, the length of the averaging time interval (time period) for this case, varying injection duration, still needs to be chosen. In order to have a fair comparison between different injection durations, the time period was selected to be 2.0 ms, which is equal to the longest injection duration, although the results are insensitive to this choice of time period.

Figure 10 shows the SMD values as a function of ambient pressures, recorded in region C (see Figure 2) and at two injection pressures (150 bar in (a) and 100 bar in (b)). The filled markers (blue and teal) show the values when injection duration was set to last for 1.0 ms, while the hollow ones (red and orange) refer to an injection duration of

2.0 ms. Again, for the same test condition, a decrease of SMD values at higher ambient pressure is observed.

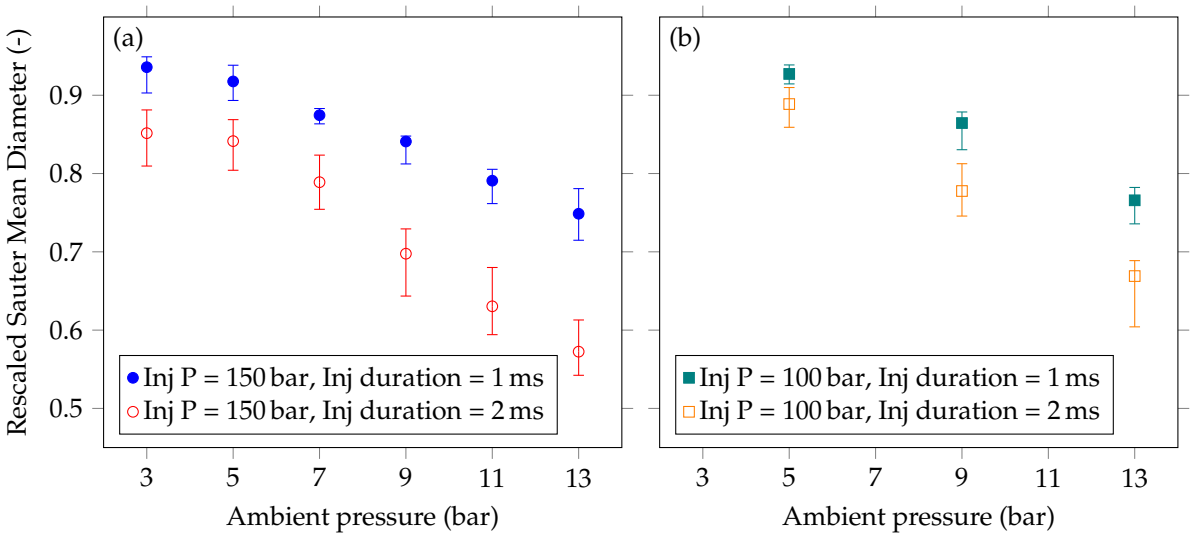

Figure 10. Rescaled Sauter Mean Diameter measured at different injection duration as a function of ambient pressures at two injection pressures—(**a**) at 150 bar and (**b**) at 100 bar. All the measurements were taken in region C (Runs 19–36 in Table 1). The markers show the median value of 20 consecutive shots, and the error bars bound the middle two quartiles.

The injection duration has a profound effect on the droplet sizes observed However, to perform the time-based average, the length of the at a given place and time in our measurements. In Figure 10a, the SMD values reduced by at least 0.09 at all ambient pressures when injection duration was doubled and by a value of around 0.2 at the highest injection pressures. This potentially resulted from the interaction between the spray plume and ambient gas. When the high speed plume enters the quiescent chamber, it induces a shear flow along its penetration direction and also vortices outside of the shear flow, promoting the ambient gas to intrude and mix with the spray plume and enhancing the droplet breakup. The extent of ambient gas entrainment in the spray plume would be a function of the duration of such an entrainment. When the injection duration is longer, more ambient gas is mixed with the droplets at the outer edge of the spray plume, causing more breakup to occur, and hence leads to a smaller SMD value. At higher ambient pressures, the density of the ambient gas is higher, so more mass of air is entrained, again leading to more breakup and smaller SMD values.

Additionally, the extent of ambient gas entrainment is also a function of the relative speed between the spray plume and the gas (dominated mainly by the injection and ambient pressures). This hypothesis can be further confirmed by checking the SMD values recorded at a lower injection pressure (Figure 10b). Although the injection duration still has a large influence on the SMD values, the difference between the 1 ms injection (teal filled squares) and the 2 ms injection (orange hollow squares) is much smaller than the one at higher injection pressures, showing that the extent of ambient gas entrainment in the spray is less sensitive to the injection duration when the injection pressure is lower. The lower spray plume momentum at 100 bar results in weaker vortex generation and less efficient gas entrainment over time hence leading to a smaller difference in SMD observed at this lower injection pressure.

In an internal combustion engine application, the injection duration depends on the amount of fuel needed and hence may not be a tunable variable. However, the current study inside a quiescent chamber with a variable injection duration indicates that the ambient gas entrainment induced by the spray already has a strong effect on droplet sizes.

In a real internal combustion engine, the ambient gas motion is much more significant and so the induced entrainment effect will be different [33].

4. Conclusions

The droplet size of liquid anhydrous ammonia sprays from a multi-hole injector was experimentally studied using the laser diffraction method in a constant volume chamber filled with nitrogen gas. The ambient (chamber) pressure spanned a wide range from 3-13 bar in increments of 2 bar, passing through the saturation pressure of ammonia at chamber temperature (8.5 bar), hence covering both flash-boiling and non-flash boiling conditions. Droplet size measurement was undertaken at three different locations relative to the injector tip – at the center of the spray (Location A), at the outer edge of the spray (Location B), and near the spray tip along the spray center line (Location C). The injector was operated at two injection pressures (100 bar and 150 bar) and under two injection durations (1.0 ms and 2.0 ms). The following conclusions are drawn:

1. The un-scattered light measured by the Spraytec provides a good indication of whether and when the bulk of the spray has entered the respective measurement locations.
2. The spray from this injector showed a drag-induced breakup dominant behaviour at different ambient pressures. When ambient pressure is higher, the Sauter Mean Diameter (SMD) at all locations are lower due to the enhanced breakup process caused by higher drag. However, such a trend was less obvious at low ambient pressures (below 5 bar), as under these flash boiling conditions, strong flash-evaporation starts to take over and become more dominant in the droplet formation process.
3. Due to the stronger interaction with the ambient gas, and hence higher drag-induced breakup, the droplets near the spray tip and at the outer edge of the spray are generally smaller than the ones at the centre of the spray.
4. Injection pressure has a moderate effect on droplet size. A higher injection pressure enhances the drag-induced droplet breakup and generally leads to a smaller droplet size. Such an effect was more clearly observed near the spray plume tip and at higher ambient pressures. Also, the difference in droplet sizes caused by injection pressures is increased when the ambient pressure is higher, owing to the stronger interaction between ambient gas and the spray under these high-drag conditions.
5. Injection duration has a significant effect on droplet size. A longer injection duration leads to stronger ambient gas entrainment and thus promotes droplet breakup and evaporation, leading to a lower SMD value. The current study in a quiescent chamber suggests that the flow induced by the spray alone is enough to reduce the resulting droplet sizes significantly, and the air motion within the combustion chamber of a thermal propulsion system is expected to have an even stronger effect due to higher flow velocities in these systems [34].

This study gives further insights into the mechanisms of spray breakup, which lead to different spray particle sizes (SMD), under different conditions – notably flash boiling and non-flash boiling. The effects of injection pressure and injection duration on SMD are further understood.

Author Contributions: Conceptualization, L.S.; Data curation, L.S. and F.L.; Formal analysis, L.S.; Funding acquisition, F.L.; Investigation, L.S.; Methodology, L.S.; Project administration, L.S. and F.L.; Software, L.S.; Supervision, F.L.; Validation, L.S. and F.L.; Visualization, L.S.; Writing—original draft, L.S.; Writing—review & editing, F.L. All authors have read and agreed to the published version of the manuscript.

Funding: This research was funded in whole or in part by Engineering & Physical Sciences Research Council (EPSRC, EP/V04673X/1). For the purpose of Open Access, the authors have

Data Availability Statement: Data supporting this paper is available from the "Oxford Research Archive" repository, accessible at https://ora.ox.ac.uk, accessed on 10 March 2026.

Acknowledgments: The authors would like to thank David L.S. Hung from Shanghai Jiao Tong University for valuable comments and discussions in relation to this work. During the preparation of this work the authors used ChatGPT 5 in order to assist with formatting the data and proofreading the manuscript. After using this tool, the authors reviewed and edited the content as needed and take full responsibility for the content of the published article.

Conflicts of Interest: The authors declare no conflicts of interest.

Abbreviations

The following abbreviations are used in this manuscript:

aSOI	after Start of Injection
GDI	Gasoline Direct Injection
LED	Light Emitting Diode
PDIA	Particle Droplet Image Analysis
PDPA	Phase Doppler Particle Analyzer
SMD	Sauter Mean Diameter

References

1. Faber, J.; Hanayama, S.; Zhang, S.; Pereda, P.; Comer, B.; Hauerhof, E.; Schim van der Loeff, W.; Smith, T.; Zhang, Y.; Kosaka, H.; et al. *Fourth IMO GHG Study 2020 (Full Report)*; International Maritime Organization: London, UK, 2021.
2. Valera-Medina, A.; Xiao, H.; Owen-Jones, M.; David, W.I.; Bowen, P.J. Ammonia for power. *Prog. Energy Combust. Sci.* **2018**, *69*, 63–102. [CrossRef]
3. Senecal, K.; Leach, F. *Racing Toward Zero: The Untold Story of Driving Green*; SAE International: Warrendale, PA, USA, 2021.
4. The National Institute of Standards and Technology. *NIST Chemistry WebBook*; NIST Standard Reference Database Number 69; NIST: Gaithersburg, MD, USA, 2023. [CrossRef]
5. Van Itterbeek, A.; Verbeke, O.; Theewes, F.; Staes, K.; De Boelpaep, J. The difference in vapour pressure between normal and equilibrium hydrogen. Vapour pressure of normal hydrogen between 20K and 32K. *Physica* **1964**, *30*, 1238–1244. [CrossRef]
6. The Royal Society. *Ammonia: Zero-Carbon Fertiliser, Fuel and Energy Store*; Policy Briefing; The Royal Society: London, UK, 2020.
7. Ambalakatte, A.; Cairns, A.; Geng, S.; Varaei, A.; Hegab, A.; Harrington, A.; Hall, J.; Bassett, M. Experimental Comparison of Spark and Jet Ignition Engine Operation with Ammonia/Hydrogen Co-Fuelling. In *Proceedings of the WCX SAE World Congress Experience, Detroit, MI, USA, 16–18 April 2024*; SAE International: Detroit, MI, USA, 2024. [CrossRef]
8. Min, C.K.; Lee, S.W.; Baek, H.K. Development of Ammonia Direct Injection 4-Cylinder Spark-Ignition Engine. In *Proceedings of the WCX SAE World Congress Experience, Detroit, MI, USA, 16–18 April 2024*; SAE International: Detroit, MI, USA, 2024. [CrossRef]
9. Reggeti, S.A.; Kane, S.P.; Northrop, W.F. Hydrogen production in ammonia-fueled spark ignition engines. *Appl. Energy Combust. Sci.* **2023**, *14*, 100136. [CrossRef]
10. Zhang, Z.; Li, T.; Chen, R.; Wang, N.; Wei, Y.; Wu, D. Injection characteristics and fuel-air mixing process of ammonia jets in a constant volume vessel. *Fuel* **2021**, *304*, 121408. [CrossRef]
11. Stone, R. *Introduction to Internal Combustion Engines*, 4th ed.; Red Globe Press: London, UK, 2012.
12. Leach, F.; Ismail, R.; Davy, M.; Weall, A.; Cooper, B. Comparing the Effect of Fuel/Air Interactions in a Modern High-Speed Light-Duty Diesel Engine. In *SAE Technical Paper*; SAE: Warrendale, PA, USA, **2017**. [CrossRef]
13. Pelé, R.; Mounaïm-Rousselle, C.; Bréquigny, P.; Hespel, C.; Bellettre, J. First Study on Ammonia Spray Characteristics with a Current GDI Engine Injector. *Fuels* **2021**, *2*, 253–271. [CrossRef]
14. Cheng, Q.; Ojanen, K.; Diao, Y.; Kaario, O.; Larmi, M. Dynamics of the Ammonia Spray Using High-Speed Schlieren Imaging. *Sae Int. J. Adv. Curr. Pract. Mobil.* **2022**, *4*, 1138–1153. [CrossRef]
15. Colson, S.; Yamashita, H.; Oku, K.; Somarathne, K.D.K.A.; Kudo, T.; Hayakawa, A.; Kobayashi, H. Study on the effect of injection temperature and nozzle geometry on the flashing transition of liquid ammonia spray. *Fuel* **2023**, *348*, 128612. [CrossRef]
16. Shen, L.; Leach, F. An experimental study on the macroscopic behaviours of ammonia sprays in a constant volume chamber. *Int. J. Hydrogen Energy* **2025**, *126*, 386–395. [CrossRef]

17. Fang, Y.; Ma, X.; Zhang, Y.; Li, Y.; Zhang, K.; Jiang, C.; Wang, Z.; Shuai, S. Experimental Investigation of High-Pressure Liquid Ammonia Injection under Non-Flash Boiling and Flash Boiling Conditions. *Energies* **2023**, *16*, 2843. [CrossRef]
18. Zhong, W.; Chen, J.; Li, C.; Huang, Y.; Pachiannan, T.; Jiang, Z.; Yuan, Y.; He, Z. Visualization study on flash boiling spray characteristics of high-pressure liquid ammonia with different nozzle diameters. *Fuel* **2024**, *367*, 131525. [CrossRef]
19. Shen, L.; Leach, F. Effect of Ambient Pressure on Ammonia Sprays Using a Single Hole Injector. *Sae Int. J. Adv. Curr. Pract. Mobil.* **2025**, *7*, 583–598. [CrossRef]
20. Zembi, J.; Battistoni, M.; Pandal, A.; Rousselle, C.; Pelè, R.; Brequigny, P.; Hespel, C. Numerical study of ammonia spray with a GDI engine injector. *J. Ammon. Energy* **2023**, *1*, 59–73. [CrossRef]
21. Liu, Y.; Zhang, H.; Yu, H.; Yan, G.; Yan, J.; He, X. Study on the macroscopic and microscopic characteristics of flash boiling spray of liquid ammonia. *Fuel* **2026**, *408*, 137696. [CrossRef]
22. Liu, X.; Zeng, G.; Yao, X.; Tang, C.; Huang, Z. Microscopic characteristics study of liquid ammonia spray under different flash boiling conditions. *Fuel* **2025**, *401*, 135869. [CrossRef]
23. Liu, X.; Yao, X.; Wang, Z.; Tang, C. Single hole ammonia spray macroscopic and microscopic characteristics at flare and transition flash boiling regions. *Appl. Therm. Eng.* **2023**, *235*, 121443. [CrossRef]
24. Mohd Murad, S.H.; Camm, J.; Davy, M.; Stone, R.; Richardson, D. Spray Behaviour and Particulate Matter Emissions with M15 Methanol/Gasoline Blends in a GDI Engine. In Proceedings of the SAE 2016 World Congress and Exhibition, Detroit, MI, USA, 12–14 April 2016. [CrossRef]
25. Leach, F.; Stone, R.; Fennell, D.; Hayden, D.; Richardson, D.; Wicks, N. Predicting the particulate matter emissions from spray-guided gasoline direct-injection spark ignition engines. *Proc. Inst. Mech. Eng. Part D J. Automob. Eng.* **2017**, *231*, 717–730. [CrossRef]
26. Malvern Instruments Ltd. *Spraytec User Manual*; Malvern: Worcestershire, UK, 2007.
27. Sauter, J. *Die Grössenbestimmung der im Gemischnebel von Verbrennungskraftmaschinen Vorhandenen Brennstoffteilchen [The Determination of the Size of the Fuel Particles Present in the Mixture Mist of Internal Combustion Engines]*; VDI-Verlag (VDI Publishing House): Berlin, Germany, 1926. (In German)
28. Pacek, A.W.; Man, C.C.; Nienow, A.W. On the Sauter mean diameter and size distributions in turbulent liquid/liquid dispersions in a stirred vessel. *Chem. Eng. Sci.* **1998**, *53*, 2005–2011. [CrossRef]
29. Kowalczuk, P.B.; Drzymala, J. Physical meaning of the Sauter mean diameter of spherical particulate matter. *Part. Sci. Technol.* **2016**, *34*, 645–647. [CrossRef]
30. Triballier, K.; Dumouchel, C.; Cousin, J. A technical study on the Spraytec performances: Influence of multiple light scattering and multi-modal drop-size distribution measurements. *Exp. Fluids* **2003**, *35*, 347–356. [CrossRef]
31. Preussner, C.; Döring, C.; Fehler, S.; Kampmann, S. *GDI: Interaction Between Mixture Preparation, Combustion System and Injector Performance*; Technical Report, SAE Technical Paper; SAE: Warrendale, PA, USA, 1998.
32. Li, X.; Wang, S.; Yang, S.; Qiu, S.; Sun, Z.; Hung, D.L.; Xu, M. A review on the recent advances of flash boiling atomization and combustion applications. *Prog. Energy Combust. Sci.* **2024**, *100*, 101119. [CrossRef]
33. Baker, S.; Fang, X.; Shen, L.; Willman, C.; Fernandes, J.; Leach, F.; Davy, M. Dynamic mode decomposition for the comparison of engine in-cylinder flow fields from particle image velocimetry (PIV) and Reynolds-averaged Navier–Stokes (RANS) simulations. *Flow Turbul. Combust.* **2023**, *111*, 115–140. [CrossRef]
34. Baker, S.J.; Fang, X.H.; Barbato, A.; Breda, S.; Magnani, M.; Fontanesi, S.; Leach, F.C.P.; Davy, M.H. Extracting vector magnitudes of dominant structures in a cyclic engine flow with dimensionality reduction. *Phys. Fluids* **2024**, *36*, 025131. [CrossRef]